# Potential-Energy and Differential-Stopping-Power Functions from Energy-Loss Spectra of Fast Ions Channeled in Gold Single Crystals*

S. Datz, C. D. Moak, T. S. Noggle, B. R. Appleton, and H. O. Lutz†
*Oak Ridge National Laboratory, Oak Ridge, Tennessee 37830*
(Received 23 October 1968)

Structure has been observed in the energy-loss spectrum of ions channeled between low-index planes in thin Au single crystals. It is proposed that the cause of this structure lies in the nature of the transverse oscillations of the ion in the interplanar potential. The particle's motion is characterized by an anharmonic oscillation; the wavelength is a function of the amplitude, and each amplitude is characterized by an energy loss. With narrowly collimated beams and small-angle detector, only particles having an integral number of wavelengths within the crystal are detected. Measurement of the wavelengths gives information about the interplanar potential. The dependence of energy loss on amplitude gives a mapping of the stopping power in the channel. Various features of the model are tested and quantitative measurements for 3-MeV $^4$He ions and 60-MeV $^{127}$I are given. Correlations with atomic parameters are discussed.

## I. INTRODUCTION

When energetic ions enter a crystal lattice with small angles to lattice rows or planes, they undergo a set of correlated small-angle collisions which tend to confine their motion so as to avoid close collisions with lattice atoms. This effect, called "channeling," was first anticipated by Stark and Wendt[1] in 1912 and rediscovered in the computer calculations of Robinson and Oen[2] on the ranges of multi-keV ions in copper and has been amply verified in a host of ion penetration experiments and theoretical treatments which have been summarized in recent reviews.[3–5] Lindhard[4] showed that at sufficiently high velocities an ion approaching a row of atoms, within a certain critical angle, experiences a continuous scattering potential made up of a sum of the individual interatomic potentials (string model). Similarly, Erginsoy[6] demonstrated that densely packed atomic planes present a uniform sheet potential to a penetrating ion.

The trajectory of ions channeled between crystal planes is governed by their interaction with the interatomic potentials of the atoms making up the plane, and the energy loss of channeled ions should depend upon the detailed stopping power (i.e., electron density and inelastic scattering cross section) it has encountered along its path.

In a previously reported experiment,[7,8] surface-barrier solid-state detectors were used to measure the energy loss suffered by high-energy (20–80 MeV) $^{79}$Br and $^{127}$I ions upon passing through oriented, thin single crystals of gold. It was found that, for incidence along low-index axial directions in the crystal, almost all the ions suffered energy losses which were significantly lower than those entering in a random direction. Low-index crystal planes were also shown to be effective in channeling. In another experiment,[9] in which time-of-flight techniques were used to improve the energy resolution, detailed angular scans were made across planar channels. Additional sharp energy-loss groups were discovered between the normal and lowest energy-loss components.

Further experiments with 60-MeV $^{127}$I ions confirmed these observations, and it was demonstrated that the energy-loss spectrum of $\alpha$ particles (3 MeV) displayed the same features.[10,11] We proposed that the explanation of this structure was to be found in the nature of the transverse oscillation of the particle in the channel and that the energy losses associated with a given wavelength and amplitude of motion would allow a mapping of the stopping power in the channel and permit the determination of interatomic potentials. In the present paper we describe several experiments which were designed to test various features of the model and present quantitative measurements which have been

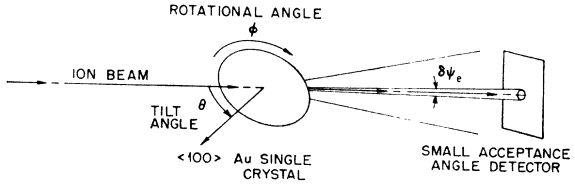


FIG. 1. Schematic of the general experimental arrangement.

* Research sponsored by the U. S. Atomic Energy Commission under contract with Union Carbide Corporation.

† Present address: Max-Planck Institute für Kernphysik, Heidelberg, Germany.

[1] J. Stark and G. Wendt, Ann. Physik **38**, 921 (1912); J. Stark, Physik Z. **13**, 973 (1912).

[2] M. T. Robinson and O. S. Oen, J. Appl. Phys. Letters **2**, 30 (1963); Phys. Rev. **132**, 2385 (1963).

[3] S. Datz, C. Erginsoy, G. Leibfried, and H. O. Lutz, Ann. Rev. Nucl. Sci. **17**, 129 (1967).

[4] J. Lindhard, Kgl. Danske Videnskab. Selskab, Mat.-Fys. Medd. **34**, No. 14 (1965).

[5] A. F. Tulinov, Usp. Fiz. Nauk **87**, 585 (1965) [English transl.: Soviet Phys.—Usp. **8**, 864 (1966)].

[6] C. Erginsoy, Phys. Rev. Letters **15**, 360 (1965).

[7] S. Datz, C. D. Moak, and T. S. Noggle, Phys. Rev. Letters **15**, 254 (1965).

[8] S. Datz, C. D. Moak, and T. S. Noggle, Nucl. Instr. Methods **38**, 221 (1965).

[9] S. Datz, H. O. Lutz, C. D. Moak, T. S. Noggle, L. C. Northcliffe, and H. W. Schmitt, Bull. Am. Phys. Soc. **11**, 126 (1966).

[10] H. O. Lutz, S. Datz, C. D. Moak, and T. S. Noggle, Phys. Rev. Letters **17**, 285 (1966).

[11] Structure in the energy-loss spectrum of 800-keV $^4$He ions has been observed by W. M. Gibson, J. B. Rasmussen, P. Ambrosius-Olesen, and C. J. Andreen, Can. J. Phys. **46**, 551 (1968).

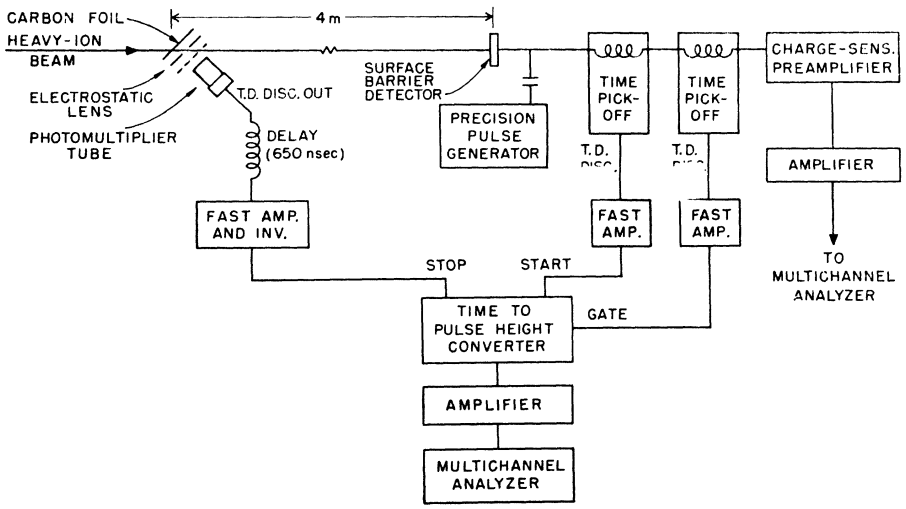


FIG. 2. Schematic of the time-of-flight energy-analysis system.

correlated with atomic parameters by the methods described by Robinson.[12]

## II. EXPERIMENTAL

The over-all experimental arrangement is pictured in Fig. 1. A beam of ions was narrowly collimated to $<0.05°$, passed through an oriented thin single crystal of gold, and the energy spectrum of the ions emerging into the acceptance angle of the analyzer ($\delta\psi \simeq 0.01°$) was recorded. The Au single crystal was mounted in a goniometer, which permitted rotation about two orthogonal axes. Tilt about an axis lying in the plane of the specimen face $\theta$ not only changed the crystallographic direction but also changed the path length of the ion in the crystal. When coupled with a rotation about an axis perpendicular to the surface, any desired $\langle hkl \rangle$ direction in the {100} projection could be achieved up to $\theta_{max} = 60°$. For the planar channels under study here, the effective path length through a {100} planar channel could be varied by a factor of 2 ($\theta = 0$–$60°$) and the {111} channel by a factor of 1.52 ($\theta = 35.2$–$60°$). Suitable adjustment of $\theta$ and $\Phi$ could also effectively tilt the planar axis with respect to the incident beam direction. Final orientation of the crystal *in situ* was aided by the observation of transmission spot patterns[13] on a fluorescent screen which could be inserted behind the crystal. Optical measurements and experience in the study of energy-loss spectra indicate that the goniometer can measure and reproduce specimen settings to better than $\pm 0.02°$. In this work we have used multicomponent beams of $^{127}$I ions with energies ranging from 20 to 100 MeV,[12] single-component $^{127}$I-ion beams at 60 and 40 MeV, and 3-MeV $^{4}$He-ion beams. All were obtained from the Oak Ridge Tandem Van de Graaff Accelerator. Beam-energy spreads were in all cases less than 2 keV.

We have used several methods for energy detection. The time-of-flight method used to detect heavy ions is illustrated in Fig. 2 and is similar to that described by Williams *et al.*[14] for studies of fission fragment mass-energy studies. The particle emerging from the gold crystal passes through a thin carbon foil, secondary electrons ejected from the back of the foil are accelerated into a plastic scintillator, and the accompanying pulse observed in the photomultiplier acts as a delayed stop pulse for a time–to–pulse-height converter. The start pulse is created when the particle strikes a surface-barrier solid-state detector at the end of a 4-m path. The limitation of time resolution was found to be in the energy straggling accompanying the passage of the particle through the thin carbon foil. When 3 $\mu$g/cm$^2$ carbon foils were used, time resolution of $\pm 0.9$ nsec was achieved corresponding to a $\Delta E/E$ of 0.0047 for 60-MeV I ions.

Magnetic analysis coupled with a position-sensitive detector[15] gave almost as good energy resolution for 60-MeV I. However, magnetic deflection separates the emerging ion charge states so that only a fraction of the emergent beam can be observed during any single run, and smoothing operations required to remove structure introduced by nonuniformities in the position-sensitive detector lowered the effective resolution by a factor of almost 2. Presently available position-sensitive detectors also have an uncorrelated noise of 50–75 keV which does not seriously affect measurements with 40–60-MeV I ions, but it is sufficient to cause deleterious effects on the 3-MeV He-ion spectra.[10]

The He-ion energy-loss spectra reported in this paper were obtained with an ordinary silicon surface-barrier detector with a resolution of 28 keV for 5.48-MeV $^{241}$Am $\alpha$ particles.

[12] M. T. Robinson, following paper, Phys. Rev. **179**, 327 (1969).
[13] T. S. Noggle, C. D. Moak, H. O. Lutz, and S. Datz, Bull. Am. Phys. Soc. **11**, 177 (1966).
[14] C. W. Williams, W. E. Kiker, and H. A. Schmitt, Rev. Sci. Instr. **35**, 1116 (1964).
[15] Nuclear Diodes, Inc., Chicago, Illinois.

### A. Crystal Preparation

Single-crystal gold films were made by vacuum evaporation and epitaxial growth on cleavage surfaces of NaCl. The detailed procedure followed closely that described by Bassett and Pashley[16] and involved the initial evaporation of about 0.25 $\mu$ of Ag onto NaCl crystals held at 300°C, followed by evaporation of gold to the desired thickness. Transfer of the gold films to gold-specimen disks employs a collodion membrane and is described as follows: Collodion membranes are made by placing several drops of collodion[17] on the surface of water. The thickness of the film formed is determined by the amount and concentration of collodion solution and size of dish used. The best thickness is established by trial and error. The film formed after the solvent has evaporated is picked up on a metal ring and stretched taut by slipping the film on the ring until wrinkles are eliminated. After water picked up with the film has dried, the membrane adheres tightly to the ring which serves as a handle for subsequent processing and mounting of the gold film.

The collodion membrane is softened by exposure to amyl acetate vapor in a closed dish until surface tension has retensioned the membrane. A gold-film specimen on the Ag and NaCl substrate is placed in the center of the membrane; upon removal from the solvent vapor the collodion adheres to the gold film and holds it while the NaCl is dissolved away with a gentle stream of distilled water, and then the silver is dissolved by dropwise application of 25–50% $HNO_3$. After thorough washing and drying, the gold film is stretched over the aperture in a gold-specimen disk. Mechanical attachment of the film to the disk is aided by previous etching of the disk in aqua regia to give a uniform microroughness, and the use of a smooth stylus to press the film into more intimate contact with the disk. A small pointed stick moistened with amyl acetate is used as a knife to cut the collodion at the periphery of the disk, freeing the specimen and disk from the membrane. The collodion on the specimen is eliminated by heating the specimen in air. It has been found that the best results are obtained by rapid heating of the specimen to a temperature in excess of 450°C and holding 3–5 min at temperature. A lower burn-off temperature is apt to leave a carbon residue, and too slow a heating rate leads to softening and melting up of the collodion before ignition and frequently leads to wrinkling of the specimen.

This procedure has proven to be a reliable method of producing essentially wrinkle-free films both for relatively large area (3-mm diam) and small area ($\frac{1}{2}$–1-mm diam) specimens. In general, it is preferable to employ the thinnest collodion membrane that will reliably withstand the softening treatment and/or exert sufficient traction to hold the gold film flat after dissolution of the substrate. In some instances, nonuniform traction on the film leads to wrinkles upon removal of the substrate materials. These can usually be eliminated by recycling the membrane with attached gold film through amyl acetate vapor; the combination of surface tension when the membrane is softened and subsequent shrinkage upon loss of solvent retensions the membrane and stretches the gold film taut.

[16] G. A. Bassett and D. W. Pashley, J. Instr. Methods 87, 449 (1959).

[17] Flexible Collodion, J. T. Baker Chem. Co., Philadelphia, Pa. As received, this material contains ethyl ether as one of its solvents and will not produce uniform films. The ether is allowed to evaporate, and amyl acetate is added to bring the solution back to original volume before using for preparation of film membranes.

### B. Specimen Characterization

The specimens used in the studies of energy loss were 12-mm diam gold disks, $\frac{1}{2}$ mm thick with 3-mm apertures over which the single-crystal film specimens were mounted. The NaCl substrate leads to (001)-oriented films which contain a high density of defects (dislocations and microtwins) as well as departures from planar geometry due to offsets in the films which occur at cleavage steps on the substrate.

Electron-microscope (EM) observations were made on companion specimens (3-mm diam disks with $\frac{1}{2}$-mm apertures) handled identically with the channeling specimens. The EM observations indicate a high density of defects in the as-grown films, i.e., $10^9$–$10^{10}$ dislocations/cm$^2$ and microtwins which occupy 1–2% of the specimen volume. Annealing above 600°C leads to substantial reduction in the size and number of twins, but relatively little reduction in the dislocation density. The EM observations were used to select films of low initial defect density and to guide and to evaluate the annealing of specimens. The combination of time and temperature employed in the annealing depends somewhat on film thickness. For films thicker than ~0.25 $\mu$, a standard schedule of 2 h (in air) at 650°C, furnace cool (initial cooling rate ~200°C/h) was employed. This schedule represents a compromise in that the growth of holes in the film (due to particulate material on substrate surface during evaporation) is essentially negligible, yet the twin volume is reduced by a factor of 5 or more. Longer times or higher temperatures can lead to complete elimination of the twins; however, little effect is normally noted on dislocation densities. The dislocations tend to tangle and lead to discrete defect-free crystal regions approximately 0.5 $\mu$–1.0 $\mu$ in diam which are misoriented slightly from adjacent regions. This leads to a structure that approximates what is commonly termed a "mosaic" structure.

X-ray rocking curves made on the channeling specimens in a parallel double-crystal spectrometer have been taken as the primary criterion of the crystal perfection of the specimens. It is believed that this provides the best characterization of the specimens, since the x-ray beam samples an area about 0.25×2 mm, an area comparable to the size of ion beams employed in the channeling studies. Rocking curves obtained in the earlier stages of these studies were typically 10–15′ [full width at half-maximum (FWHM)], whereas the

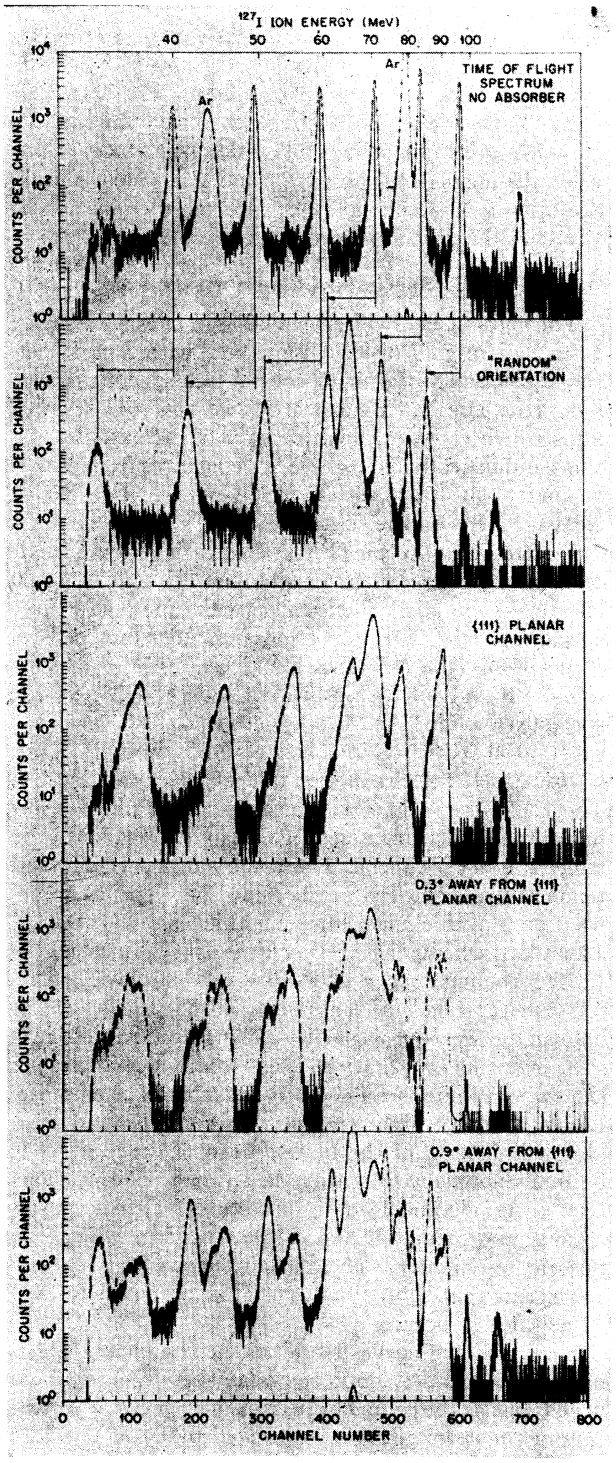


FIG. 3. Time-of-flight energy-loss spectra with multicomponent $^{127}$I beams through 0.3 $\mu$m of Au. Spectra are shown for random orientation and various tilt angles with respect to a {111} plane. The peaks labeled Ar arise from argon impurities in the stripper canal.

most recent specimens studied have been 6–7′. In addition to the rocking curves, x-ray topographs have been obtained to provide information on the uniformity with which the epitaxially established orientation is maintained over the full 3-mm diam area of a specimen. In this case, the divergence of the x-ray beam employed to obtain the topographs was 3′, and misorientations in excess of this value appeared as dark regions in the topograph (the image was formed from the diffracted beam).

The resolution in the topographs was approximately 5 $\mu$ and was incapable of resolving the mosaic structure. However, it clearly showed the effect of wrinkles and misorientation at offsets in the films and as such provides information on the precision with which the basic orientation is maintained over macroscopic dimensions. Observations of this type lead to the conclusion that in excess of 95% of the specimen volume is oriented within $\pm 1.5'$ of a common orientation; from rocking-curve measurements and the EM observations we can conclude that the distribution of misorientations resulting from structural defects and deviations from planar geometry is given by the FWHM values obtained from the x-ray rocking curves and in general relate to departures from the mean orientation of regions less than 5 $\mu$ in size.

Determination of specimen thickness has been made by weighing of the aperture plates before and after mounting of the film. A Mettler microbalance was employed with a sensitivity of $\pm 2\frac{1}{2}$ $\mu$g. Because most of the films mounted led to weight changes in excess of 250 $\mu$g, the average specimen mass thickness was determined to better than 1%. Thickness determinations from several arrays of vapor-deposited specimens indicated a maximum systematic change in thickness of less than 0.3%/mm.

The foregoing discussion of the characterization of the specimens employed in this work is believed to be important for the following reasons. First, it is recognized that departures from crystal perfection affect the channeling process. It is not clear as to the detailed effects of dislocations on channeling, although the atomic displacements near the core of a dislocation must certainly lead to a perturbation of trajectories or dechanneling of ions passing sufficiently close to the dislocation lines. On the other hand, the more or less cellular nature of the dislocation distribution in the specimens employed in these studies is believed to limit the target area of the "imperfect" crystal regions to less than 5% of the specimen volume, leaving in excess of 95% of the specimen volume as "perfect" crystals with an orientation distribution given by the x-ray rocking-curve values. Secondly, it has been assumed until rather recently that the mosaic spread affects the energy-loss spectra mainly in an adverse fashion. Efforts to improve and better characterize the specimens stems from this. Recent developments in the theoretical treatment of

channeling[12] indicate the importance of characterizing the specimens in terms of the mosaic structure.

## III. RESULTS AND DISCUSSION

The first evidence of structure was observed in measurements of the energy-loss spectra of multicomponent beams[9] of $^{127}$I ions passing through planar channels in very thin gold single crystals. (In these experiments time-of-flight energy analysis was used and the detector was in line with the primary beam.) The observations are summarized in Fig. 3. Figure 3(a) shows an open multicomponent beam spectrum (no absorber), and Fig. 3(b) shows the energy loss suffered by each beam component when a gold single crystal oriented in a "random" direction is inserted in the beam. The spectrum of Fig. 3(c) was obtained when the crystal was aligned with a {111} plane. As we had noted previously in experiments using lower resolution solid-state detectors,[1] almost all of the particles observed lose considerably less energy than for a random orientation; the population at the random-loss position compared to the channeled peak is down by at least a factor of 10. More interesting is the appearance of an intermediate-energy-loss peak between the channeled and random-energy-loss positions. The relative population of the intermediate peak is considerably enhanced by tilting the crystal plane at a small angle with respect to the beam-detector line [Fig. 3(d)]. Tilting further off plane enhances the relative populations of the random-loss groups [Fig. 3(e)] but the low-loss and intermediate-loss groups are still observed.[18] Further refinement of energy and angular resolution using magnetic analysis and a position-sensitive detector led to the observation of the spectra of the type shown in Fig. 4.[10] Four distinct groups were observed, none of which corresponded to random energy loss. We proposed that the explanation of this structure lay in the detailed history of the particle as it undergoes transverse oscillations on its path through the crystal channel.

### A. First-Order Model

Consider a planar channel consisting of two parallel closely packed lattice planes (Fig. 5). In this channel a charged particle of energy $E$ experiences a repulsive force from the atoms in each wall. We assume a smooth "planar potential," $V(x)$,[6] where $x$ is the distance from the midplane. The particle motion reduces to a two-dimensional problem in which the direction of incidence into the channel lies in the xz plane. The walls are assumed to be rigid. Since for channeled particles the maximum angle between particle trajectory and the plane is $\sim 1°$,[4] the $z$ component of the velocity is assumed to be constant. Thus,

$$\frac{d^2x}{dz^2} = -\frac{1}{2E}\frac{\partial V(x)}{\partial x}, \tag{1}$$

[18] Intermediate-energy-loss groups were groups suspected in our previous work (see Fig. 7 of Ref. 8), but lack of energy resolution precluded any unambiguous identification.

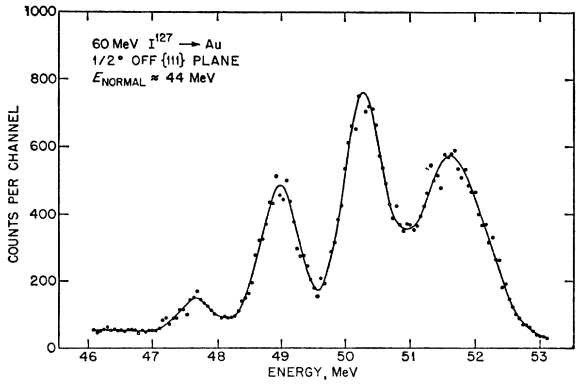


FIG. 4. Magnetic-deflection spectrum (recorded with a position-sensitive detector) of 60-MeV $^{127}$I passing through 0.7 $\mu$m of Au. The detector is in line with the beam direction and the crystal is tilted $\frac{1}{2}°$ from a {111} plane. The energy of a particle traversing the crystal in a random direction is 44 MeV.

where $E$ is the particle energy. We can express the potential, in general, in the form of a polynomial expansion

$$V(x)=V(0)+a_1x^2+b_1x^4\cdots, \tag{2}$$

in which case the equation of motion is that of an undamped anharmonic oscillator. The consequences can be seen in Fig. 6, which shows trajectories for three different impact parameters with respect to the channel midplane. Ions entering close to the midplane are deflected only weakly (path $a$); the wavelength $\lambda$ of their oscillatory motion is comparatively long and their amplitude $A$ is comparatively small. Those entering closer to the edge of the channel (paths $b$ and $c$) are repelled more strongly and have paths of larger amplitude and shorter wavelength. Assuming sinusoidal motion, we can approximate the solution by the periodic form

$$x=A_1\sin[(z-z_0)/\lambda\!\!\!^{-}]+A_3\sin[3(z-z_0)/\lambda\!\!\!^{-}], \tag{3}$$

where $A=A_1+A_3$ is the oscillation amplitude and $\lambda\!\!\!^{-}=\lambda/2\pi$. Neglecting higher-order terms in Eq. (2), we insert (3) and (2) into (1). Setting the coefficients of $\sin[(z-z_0)/\lambda\!\!\!^{-}]$ and $\sin[3(z-z_0)/\lambda\!\!\!^{-}]$ to zero yields $A_1\gg A_3$ and

$$\lambda\!\!\!^{-2}=a+\tfrac{3}{4}bA_1(A_1+A_3)\approx a+\tfrac{3}{4}bA^2, \tag{4}$$

where $a=a_1/E$ and $b=2b_1/E$. For any realistic potential

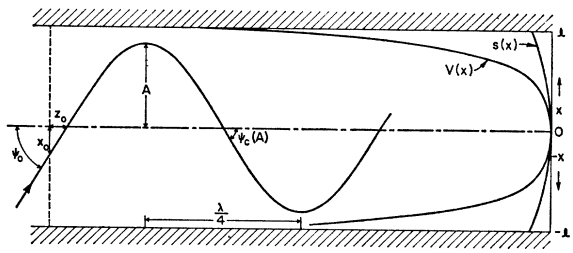


FIG. 5. Trajectory of an ion entering a planar potential at $x_0$ with angle $\psi_0$. The potential $V(x)$ and stopping power $s(x)$ functions are indicated on the right.

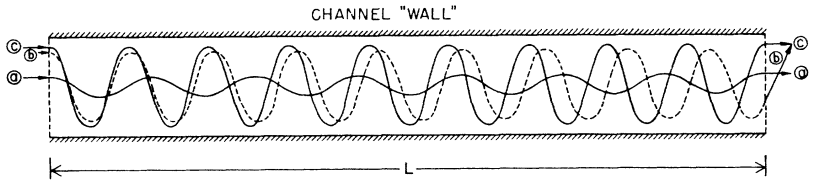


FIG. 6. Trajectories for three entrance points. Particles $a$ and $c$ will reach a detector in line with the beam.

the anharmonicity decreases with decreasing amplitude so that in the region of minimum amplitude, i.e., for parallel entrance close to the center of the channel, the wavelength should be independent of amplitude. We designate this as the $A_0$ region.

The energy loss suffered by particles in this energy range is primarily caused by inelastic collisions with electrons, and since the electron density close to the atomic planes is higher than at the channel center, the stopping power $s(x)$ increases with $x$. The energy loss of particle $b$ (Fig. 6) should be larger than that of $a$ because it has penetrated the atomic planes more deeply and more often. We can therefore associate (for a given crystal thickness) an energy loss with a trajectory and a given entrance point and hence with a given wavelength and amplitude.

As the entrance point is moved from the midplane toward the channel wall, the energy loss increases and if the energy spectrum of all the emerging particles were measured it would be structureless. However, if the detector subtends a small angular aperture, only those trajectories which leave the crystal within that angle would be detected. This introduces a boundary condition for the wavelength of the detected particles

$$\lambda_a=(L\pm z_0\mp z_e)/n\,, \tag{5a}$$

$$\lambda_b=(L\pm z_0\pm z_e)/(n+\tfrac{1}{2})\,, \tag{5b}$$

where $n$ is an integer, $L$ is the length of the crystal, and $z_0$ and $z_e$ are the lengths associated with the phase shifts of incidence angle $\psi_0$ and exit angle $\psi_e$. [For sinusoidal motion $z=\lambda\cos^{-1}(\lambda\psi/A)$.]

### B. "Perfect Crystal" Experiment

Let us first consider the information obtainable from an ideal experiment in which we employ a flawless crystal of perfectly uniform thickness. If the experiment were arranged with the detector and beam in line and the planar channel aligned with the detector beam axis, i.e., $\psi_0=\psi_e=0$, then $\lambda_a=L/n$, $\lambda_b=L/(n+\frac{1}{2})$. If the path length is changed by changing $\theta$, the wavelengths (and associated energy loss) of the detected groups shifts until at $\Delta L=L_2-L_1=\lambda$; $(dE/dz)_{n,L}=(d\sim/dz)_{(n+1),L}$ A measurement of the $\Delta L$ required to return to a given wavelength group is a direct measure of the wavelength, and the dependence of $\lambda$ upon stopping power is established. Tilting the crystal plane with respect to the beam axis (i.e., $\psi_0=\psi_e\neq 0$) splits the $\lambda_b$ solutions but the $\lambda_a$ solutions are unchanged as long as the detector is kept on the beam axis.

The population of a given group depends on the length of the region $\delta x_0$ which leads to exit angles included within the detector aperture $\delta\psi_e$. With $\psi_0=\psi_e=0$ and a fixed small aperture detector, two effects combine to suppress the intensity of high-amplitude groups. First, the variation in exit angle with entrance point $\delta\psi_e/\delta x_0$ increases with both decreasing wavelength and increasing amplitude; and, second, a steeper potential gradient at larger amplitude causes a more rapid decrease in wavelength within a given $x_0$ zone.

The amplitude of an oscillation is a function of the transverse energy,

$$V(A)=V(x_0)+E\sin^2\psi\,, \tag{6}$$

so that for each amplitude there is a cricital angle $\psi_c(A)$ corresponding to $x_0=0$ beyond which the intensity at $A$ vanishes. When the crystal is tilted, the population of a given sidegroup increases until it drops abruptly to zero at $\psi_c(A)$. Here again two effects are responsible for the increase. As $\psi$ is increased from 0 to $\psi_c(A)$ the phase shift passes from $\frac{1}{4}\lambda$ to 0 and $d\psi/dz$ goes from maximum to minimum. The second effect again is related to the steepness of the potential. As $\psi$ is increased the entrance point $x_0$ for a given $A$ is moved to smaller values and since $\partial V(x_0)/\partial x_0$ decreases with $x$, a larger range of $x_0$ values will be included in $\delta V(A)$. The width of the energy-loss group is related to the gradient of the stopping-power function within the $\delta A$ region contributing to the peak.

If the functional form of the trajectory is known, a measurement of the cutoff angle $\psi_c(A)$ for a given wavelength group would give the amplitude and the exact path is determined. For example, if the wave were sinusoidal, we should have

$$A=\lambda\psi_c(A)\,. \tag{7}$$

Even if the functional form is not known, it could be measured by an experiment in which the detection angle $(\psi_e)$ is changed to compensate for a thickness change which deflects the emergence angle for a given $dE/dz$ group; e.g., start with $L=L_1$ and $\psi_0=\psi_e=0$ and focus attention on one $dE/dz$ group. Now if the pathlength is changed slightly, the group emergence angle also changes. By rotating the detector to find the emergence angle, it could be followed up to $\psi_c(A)$. This procedure determines the detailed trajectory shape over a quarter wavelength.

### C. Imperfect Crystals

For the experiments under consideration here, we can divide crystal imperfections into two classes: those

which perturb the motion of the channeled particle (interstitial atoms, lattice vibration, etc.) and those which directly affect the observation of structure (lack of thickness uniformity and mosaic spread). Interstitial atoms can scatter a channeled ion into a random path or perturb the wavelength of an ion which remains channeled after the collision. Both of these effects tend to smear the structure by filling the valleys between peaks. If the particle is scattered into a random path after it has traversed part of the crystal, it may still be detected in the forward direction, but its total energy loss will be the sum of the channeled portion and the random portion of its path. Similarly, a particle which only suffers a perturbation in wavelength will have some intermediate energy loss for given detection conditions.

Experience obtained in a number of experiments has qualitatively verified the original observations of Nelson and Thompson[19] on the effect of radiation damage on channeling. It has been observed that the peak-to-valley ratio for a given specimen and incident beam direction deteriorates in time with exposure to the heavy ion beams which have been employed in these studies. It is estimated from the beam current and beam area that a reduction of a factor of 2 in the peak-to-valley ratio occurs for a dose of approximately $10^{12}$ ions/cm$^2$ in specimens in which the ion path length is 1 $\mu$m. This result appears consistent with the density of damage clusters observed in radiation-damage studies.[20,21] The magnitude of this effect depends to a considerable extent on the nature of the channeled ion. A light ion is much more sensitive to single scattering events since it is scattered through a larger angle than a very heavy ion incident at the same impact parameter. On the other hand, heavy ions can cause more radiation damage and thereby produce clusters of interstitial scattering centers. In accordance with the above, we have observed that the structure of channeled He-ion energy-loss spectra is much more sensitive to radiation damage than the structure with $^{127}$I ions and that prolonged bombardment with $^{127}$I ions can strongly diminish the peak-to-valley ratio.

For ion trajectories that are closely confined to the center of the channel, the effect of lattice vibrations is small since it will only be felt in the averaging over many atom collisions. Only when the amplitudes are large and the ions approach the atomic planes at distances comparable to vibrational displacements are strong perturbations felt. Here again the effect on light ions is greater than for heavy ions. The effect of thermal vibrations on the potential is discussed more fully by Robinson in the following paper.[12]

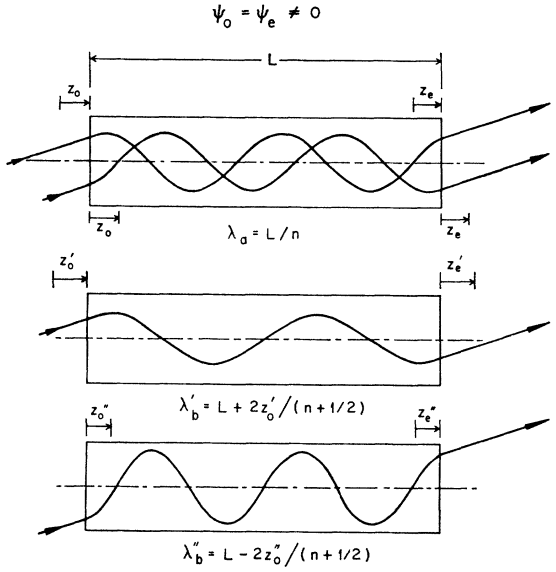


FIG. 7. Trajectories demonstrating the four solutions of Eq. (5a) and (5b) for $\psi_0 = \psi_e \neq 0$. The solutions to Eq. (5a) ($\lambda_a$) are degenerate in wavelength. The solutions for Eq. (5b) ($\lambda_b'$ and $\lambda_b''$) give wavelengths longer ($\lambda_b'$) and shorter ($\lambda_b''$) than Eq. (5a).

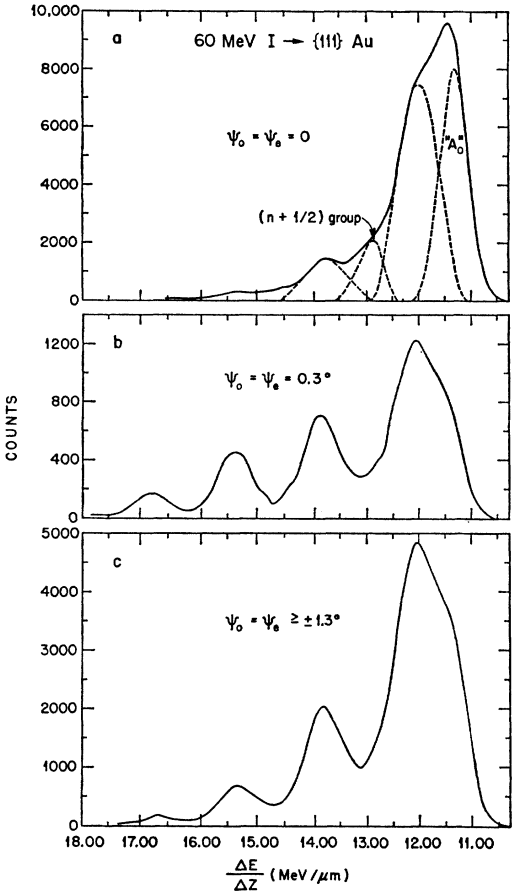


FIG. 8. Energy-loss spectra for 60-MeV $^{127}$I ions in 0.9 $\mu$m of {111} Au (time-of-flight energy analysis).

[19] R. S. Nelson and M. W. Thompson, Phil. Mag. 8, 1677 (1963); 9, 1069 (1964).
[20] T. S. Noggle and O. S. Oen, Phys. Rev. Letters 16, 395 (1966).
[21] T. S. Noggle and J. H. Barrett (unpublished).

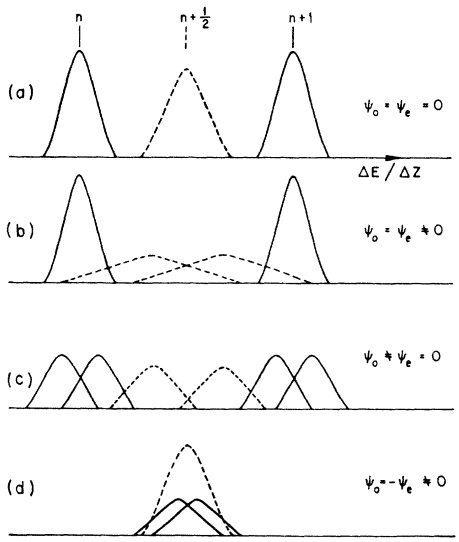


FIG. 9. Schematic representation of energy-loss spectra, expected from the model, for a crystal with a small mosaic spread. (The half-intege groups are indicated by the dashed curves.)

If the sample thickness is not uniform over the bombarded area, two effects occur which tend to cancel each other. For example, an increase in thickness will, of course, increase the energy loss of a particle on a given trajectory, but an increase in $L$ will also shift the wavelength of the focussed group to higher values [Eq. (5)] and consequently lower $\Delta E/\Delta z$ for the detected particles. The degree of compensation will depend on the shape of the stopping-power function in the channel. For channeling experiments reported here the compensation is almost complete; i.e., $\Delta E$ for a given energy-loss group is almost independent of $L$. If this compensation effect were completely absent, coherent structure could still be observed as long as the thickness was uniform to $\ll\frac{1}{4}\lambda$. The wavelengths in question in this work ($\sim 1\ \mu$m) require that $\Delta L < 0.25\ \mu$m. The crystals used ranged in thickness from 0.2 to 1.5 $\mu$m with a uniformity of $<0.3\%$ and easily met the $\frac{1}{4}\lambda$ criterion. This uniformity is difficult to achieve with thicker crystals made by etching techniques.

The effect of mosaic spread in the crystal on the spectra depends greatly on other experimental conditions and upon whether we are considering the integral solutions [Eq. (5a)] or the half-integral solutions [Eq. (5b)]. When the detector is in line with the beam direction, $\psi_0=\psi_e$ and $z_0=z_e$. For the integral solutions the phase factors cancel and the structure is unaffected by a spread in $\psi$. For the half-integral solutions the phase factors add, and slight variations in $\psi$ cause drastic changes in the transmitted wavelength. This can be visualized with the aid of Fig. 7, in which the four trajectories for the $n=2$ solutions are plotted. Mosaic spread (variation in $\psi$) is equivalent to variation in entrance and exit points. For the integral solutions a shift in entrance angle is exactly compensated by a shift in exit angle. On the other hand, with the half-integral solutions, a decrease in entrance angle causes an increase in exit angle, and since $\psi_c(A)<0.5°$, a distribution in $\psi$ of $>0.1°$ can completely eliminate the observation of structure attributable to half-integral solutions.[22]

### D. Verification of the Model

As stated earlier, when $\psi_0=\psi_e$, we should only expect to resolve the peaks corresponding to integral solutions [Eq. (5a)]. Further, it would be expected that the peak positions would be independent of $\psi$. This is demonstrated in Fig. 8, which shows the spectra obtained in a sweep across a {111} plane. In Fig. 8(c) is a single spectrum obtained by tilting the crystal in steps of 0.024° through a total angle of 1.3° on either side of the channel midplane (artificial "mosaic spread"). During this traverse, equal exposure time was spent at each angular setting. The peak positions are still easily discernible, whereas in the spectrum taken at $\psi_0=\psi_e=0$ the structure is not as well resolved. This can be understood from the expected behavior shown schematically in Figs. 9(a) and 9(b). When $\psi_0=\psi_e=0$, the half-integral solutions are merged and the effect of mosaic spread is at a minimum. The valleys between the integral solutions are then filled, and the structure is ill defined. When the

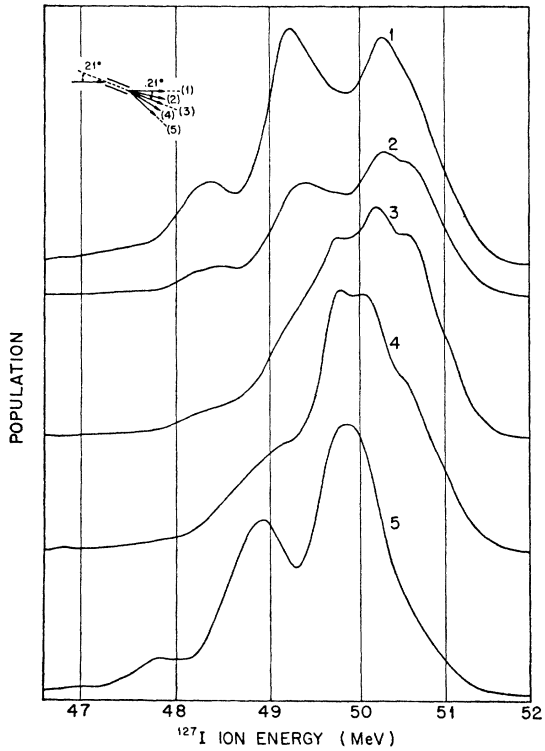


FIG. 10. Energy-loss spectra of 60-MeV $^{127}$I ions emerging from a 0.9 $\mu$m Au crystal. $\psi_0$ was 0.21° with respect to a {100} plane. $\psi_e$ was 0.21° for spectrum 1 and was varied in 0.1° steps to $\psi_e=-0.21°$ for spectrum 5.

[22] The effect of mosaic spread on the $A_0$ group has been discussed by R. von Jan, Phys. Rev. Letters 18, 303 (1967).

plane is tilted to the beam axis [Fig. 9(b)] the half-integral solutions split, the effect of mosaic spread increases, and the integral peaks are well resolved [Fig. 9(b)]. Using the peak shapes obtainable from Figs. 8(b) and 8(c) to strip the spectrum of Fig. 8(a) reveals, by difference, an additional group which corresponds in expected position to an $(n+\frac{1}{2})$ group. Remnants of half-integral groups may also be inferred on the sides of the peaks in Fig. 8(b).

Consider now the model predictions for the case of $\psi_0 \neq 0$ shown schematically in Figs. 9(b)–9(d). At $\psi_0=\psi_e$ the two solutions of Eq. (5a) are degenerate and not broadened by mosaic spread. As the detector angle is tilted so that $\psi_e$ is no longer equal to $\psi_0$ [Fig. 9(c)], the solutions become nondegenerate and the peaks split. At $\psi_0=-\psi_e$ the two half-integral solutions become degenerate and a new peak is constituted at the $(n+\frac{1}{2})$ point. [At $\psi_0=-\psi_e=\psi_c(A)$ all four solutions are degenerate at the $(n+\frac{1}{2})$ point.] This has been verified by the experimental spectra shown in Fig. 10.

The expected energy dependence of the wavelength can be obtained by integration of Eq. (1)

$$(dx/dz)^2=[V(A)-V(x)]/E \tag{8}$$

and

$$\lambda=4E^{1/2}\int_0^A dx/[V(A)-V(x)]^{1/2}, \tag{9}$$

from which $\lambda \propto E^{1/2}$. This has been confirmed by measurements of wavelength in the {111} plane with 15- and 60-MeV $^{127}$I beams. The wavelengths at 15 MeV were half as large as those obtained at 60 MeV. Further, if we make a downward change in velocity and then an upward change in thickness to compensate, it should be possible to arrive at similar spectra. The result is shown in Fig. 11. Other evidence of this trend can be adduced from Fig. 3, in which a higher number of intermediate-energy-loss groups is seen at lower incident energies.

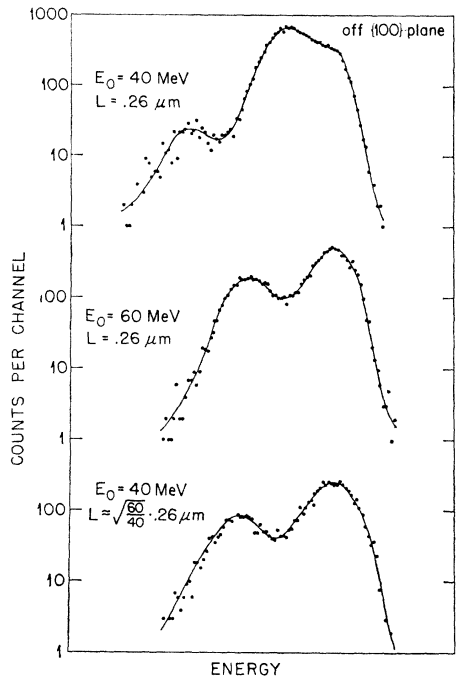


FIG. 11. Energy-loss spectra of $^{127}$I ions demonstrating the equivalence of length and velocity in determining the spectrum shape (wavelength).

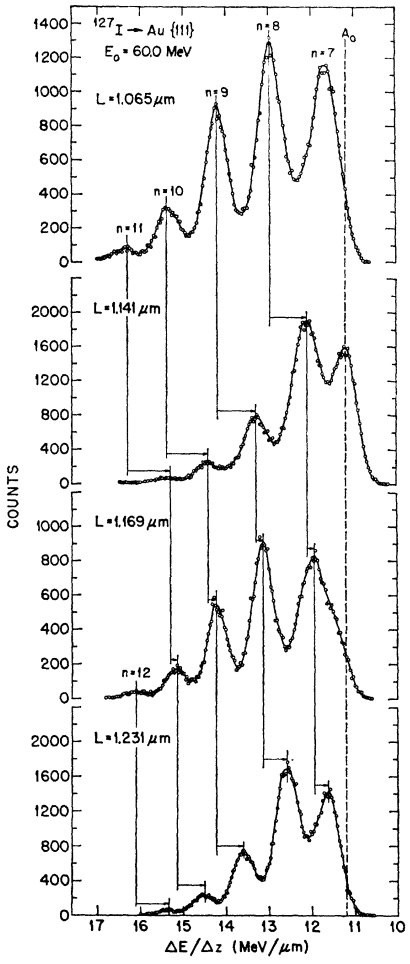


FIG. 12. Energy-loss spectra of 60-MeV $^{127}$I ions channeled in a {111} plane of Au as a function of path length (time-of-flight energy analysis).

The effect of incident-ion atomic-number $Z_1$ on $\lambda$ can be estimated if it is just assumed that $V(x)$ is reasonably represented by some form of a screened Coulomb potential, i.e.,

$$V(x)\simeq Z_1Z_2e^2f(x/a_s), \tag{10}$$

where $a_s$ is some screening radius relatively insensitive to $Z_1$ for large $Z_2$. Then for the same $Z_2$, $\lambda \propto (E/Z_1)^{1/2}$, and it would be expected that the wavelengths for 60-MeV $^{127}$I ions in Au will be approximately equal (within 20%) to those for 3-MeV $^4$He ions. This is amply borne out by the results given in the following section.

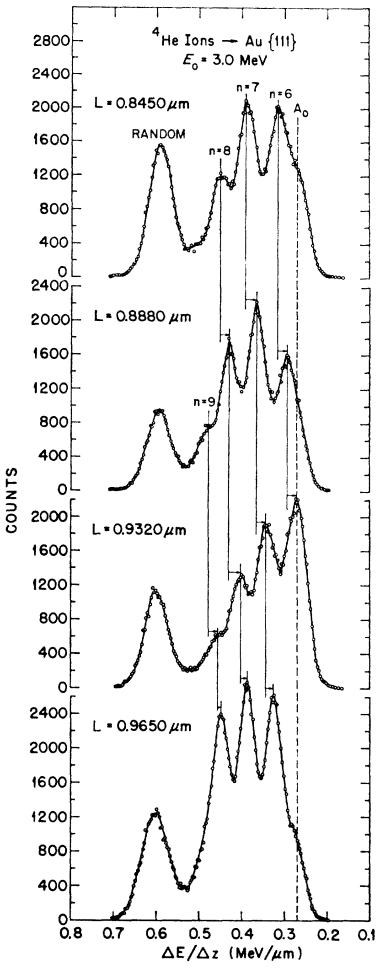


FIG. 13. Energy-loss spectra of 3-MeV $^4$He ions channeled in a {111} plane of Au as a function of path length (silicon surface-barrier-detector energy analysis).

### E. Wavelength Measurements

For the crystals used, the one feature of the spectrum which lends itself to precise measurement is the position of the peaks for the integer solutions with $\psi_0=\psi_e$. In Fig. 12 we have plotted $\Delta E/\Delta z$ spectra for $^{127}$I ions channeled in a {111} plane for several different thicknesses. Figure 13 shows similar spectra for 3-MeV He ions. (These spectra were taken at various tilt angles with respect to the plane, and no significance should be attached to the relative group populations.) The position marked $A_0$ corresponds to the minimum-energy-loss group. The particles in this group have been confined to trajectories near the channel midplane where the potential is almost harmonic. The definition of the $A_0$ group depends on the detector aperture $\delta\psi_e$; e.g., for $\psi_0=\psi_e=0$ all amplitudes having $\psi_c(A)\leq\delta\psi_e$ will be detected without regard to integral wavelength conditions. Thus, in the 1-$\mu$m wavelength region for $\psi_e\simeq 0.001$ rad, all particles with $A<0.15$ Å will be detected [see Eq. (7)]. The peak position of the $A_0$ group should not vary, and the upper right-hand leading edge of this group represents the energy loss for particle paths very close to the midplane. The position of the random-energy-loss group seen in the $^4$He-ion spectra is similarly invariant. (No significant random-energy-loss component was observed in the $^{127}$I channeling experiments.) The peaks of the intermediate groups move with changing path length as predicted by Eq. (5a). Plots of the peak positions versus $\Delta E/\Delta z$ for 60-MeV $^{127}$I and 3-MeV $^4$He ions in the {100} and {111} planar channels of Au are shown in Figs. 14 and 15. The accuracy of determining the peak positions is greatest in the middle of the $\Delta E/\Delta z$ region. At high values of $\Delta E/\Delta z$ the group populations are small and at low values it is difficult to separate a side-group peak from the $A_0$ group. Care was necessary in choosing $\theta$ so as to avoid coincidence with axial channels else the spectrum can be confused by scattering into alternative planar channels. This is especially true in the region of $\theta=45°$ (i.e., the ⟨110⟩ axis) for ⟨100⟩ crystals used. The vertical distance between lines represents the energy spacing between groups at a fixed thickness. With I ions the spacings are almost equal but for He ions there is a slight compression between groups with increasing $\Delta E/\Delta z$.

In the figures, to first order, the horizontal interval between the $n$ and $(n+1)$ groups is the wavelength of the particles in the $n$ group at the corresponding value of $\Delta E/\Delta z$ on the abscissa. Approximate values of $n$ (within one unit) can be obtained from the measured spacing at a given thickness. Actually, since the particle

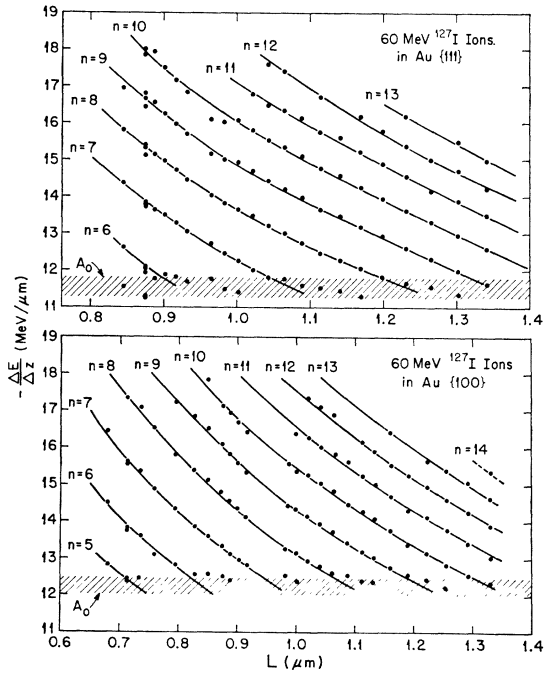


FIG. 14. Energy loss at the group peak position for 60-MeV $^{127}$I ions channeled in {111} and {100} planes of Au as a function of path length. The symbol $n$ designates the number of particle oscillations along the path.

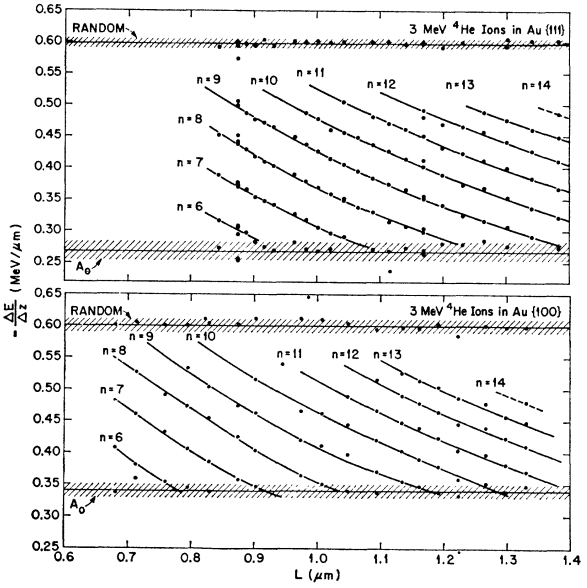


FIG. 15. Energy loss at the group peak position for 3-MeV $^4$He ions channeled in {111} and {100} planes of Au as a function of path length.

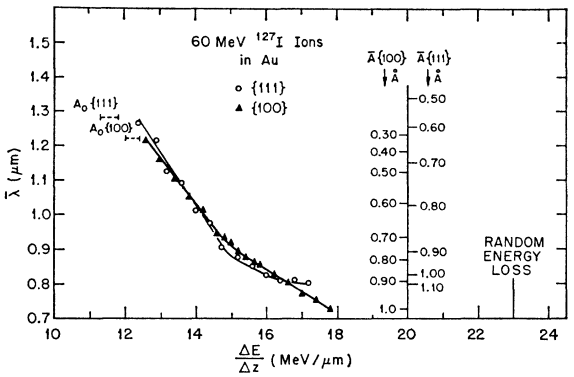


FIG. 16. Mean wavelength $\bar{\lambda}$ and amplitude $\bar{A}$ for 60-MeV $^{127}$I ions oscillating in {111} and {100} planar channels of Au as a function of stopping power $\Delta E/\Delta z$.

loses a significant fraction of its energy, its trajectory is somewhat altered so that, strictly speaking, the condition for observation is an integral number of periods. To the degree that the parallel and transverse energies are separable, there are two effects of energy loss on the path. First, since the particle is oscillating in a transverse potential with a fixed frequency, a decrease in parallel velocity will decrease the wavelength [Eq. (9)]. On the other hand, a loss in transverse energy will decrease the amplitude and increase the wavelength. For reasons which are discussed in detail by Robinson,[12] the first effect predominates and results in a slight shrinkage in horizontal spacing with increasing thickness. The $n$ values assigned to the curves are obtained from the corrected integral-period criterion.[12] The average spacings between groups, $\bar{\lambda}$, are plotted against the corresponding values of $\Delta E/\Delta z$ for 3-MeV $^4$He in Fig. 16 and for 60-MeV $^{127}$I ions in Fig. 17. As anticipated, the stopping power increases with decreasing wavelength.

## IV. CONCLUSIONS

A precise experimental mapping of the trajectory as suggested in Sec. III B was not possible because of the uncertainty in angle introduced by mosaic spread. It is possible, however, to derive a trajectory from an assumed form of the interplanar potential. In our previous communication[10] we used the planar Moliere potential[6] with the Thomas-Fermi screening length in Eq. (2) and obtained from Eq. (9) a wavelength in reasonable agreement with the measurement. Robinson has also used a modified Moliere potential of the form

$$V(x)=V_0\cosh bx, \tag{11}$$

where $b$ is the potential parameter related to an inverse screening length.

$$V_0=0.35(8\pi\rho Z_1Z_2e^2l/b)e^{-bl}, \tag{12}$$

where $\rho$ is the atomic-number density in the target and $l$ is half the interplanar spacing. Using the data available from two different interplanar spacings ({111} and {100}), he finds satisfactory agreement with the experimental data over the entire range of measurements and is able to obtain values for the $b$ parameters. The amplitudes originally derived[10] were based upon the assumption that the stopping power $s(x)$ was proportional to the electron density $d(x)$ and that $d(x)$ was connected to the potential through the Poisson relation, i.e., $\nabla^2V(x)=d(x)\propto s(x)$. From Eq. (11) it would then be anticipated that $s(x)\propto\cosh bx$. The much more extensive body of data now available demonstrates clearly

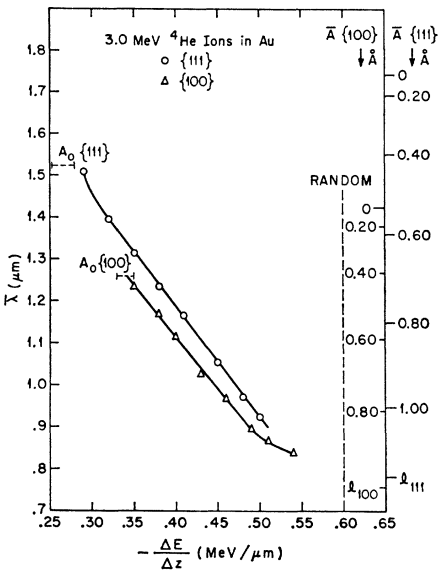


FIG. 17. Mean wavelength $\bar{\lambda}$ and amplitude $\bar{A}$ for 3-MeV $^4$He ions oscillating in {111} and {100} planar channels of Au as a function of stopping power.

that this assumption is incorrect. A more exact relationship between $V(x)$ and $s(x)$ has been derived directly from the data by Robinson, who found that the form

$$s(x) \propto \cosh \tfrac{1}{2} bx$$

fit the data very closely for both $^{127}$I and $^{4}$He ions. Thus the stopping-power function rises much more gradually in the region of the channel walls than had been assumed. This observation may reflect the fact that, at the velocities of the ions used in the experiment, nonadiabatic interactions of the ions with more tightly bound electrons are improbable. The values for the average amplitudes $\bar{A}$ given on the right-hand ordinates of Figs. 16 and 17 are obtained from Robinson's potential and stopping-power functions.

From these and Table IV in Ref. 12, it can be seen that the stopping-power measurements are applicable to a range of approach distances (with the Au atoms in the plane) between 0.1 and 0.6 Å. If we apply the criterion that to cause ionization the velocity of an ion must exceed the orbital velocity of a bound electron, we find that only $\sim$11 of the 79 Au electrons are clearly free to interact ($6s^1$ and $5d^{10}$). The 60-MeV $^{127}$I and 3-MeV $^{4}$He ions used in this study have velocities equivalent to electrons at 285 and 410 eV, respectively. The kinetic energies of the electrons in the Au $5p_{3/2}$, $5p_{1/2}$, and $4f_{7/2}$ shells are $\sim$250, 340, and 460 eV, and the shells have mean radii of 0.60, 0.55, and 0.28 Å, respectively.[23] It would appear, therefore, that in just the region probed by the experiment, the cross sections for inelastic interaction of the penetrating ion with a bound Au electron should decrease with decreasing distance of closest approach. The stopping power, which is the product of the electron density and the inelastic cross section per electron, does not increase as rapidly as the electron-density function itself.

The value of $s(x)$ gives the inelastic energy loss per unit length suffered by an atom passing at a fixed perpendicular distance from an atomic plane, averaged over individual collisions with atoms of varying azimuthal displacement in the plane. It should therefore be possible, with the aid of measurements on planes with differing spacings and planar densities, to extract the values of inelastic energy loss as a function of impact parameter relevant to single-atomic-collision processes. In principle, this information could be obtained from single-collision gas-scattering experiments in which the inelastic energy loss of the projectile is measured as a function of scattering angle.[24] However, in the high-energy region (which can be investigated by channeling experiments), the degree of inelasticity may be too small to measure with any accuracy. For example, in the two cases reported in this paper, the fractional energy loss per atomic length is of the order $\sim 10^{-4}$. Thus the disadvantage of multiple-collision studies may be counterbalanced by the multiplication of the energy loss which eases the experimental energy-resolution requirements. The case for $^{4}$He ions is relatively straightforward since at these velocities they are essentially bare nuclei. The principal difference from gas collisions would be the energy loss to plasmons which could be estimated from the stopping power at the center of the channel.[25] The case for $^{127}$I ions is considerably more complex since the charge and excitation state of the ion at the time of collision is not well defined and would require an additional averaging process. To this end it would be necessary to determine charge-state distributions of channeled ions in the medium.[26]

From the foregoing, it can be seen that the measurement of the wavelengths of ions oscillating between crystal planes gives information about the nature of the interatomic potential operative within the crystal. The resulting potential parameters are in reasonable agreement with those expected from theory. More significantly, however, direct information concerning the dependence of inelastic loss on distance from atomic planes is obtained, for which none of the present theories gives an adequate description.

## ACKNOWLEDGMENTS

It is a pleasure to acknowledge H. A. Schmitt for his aid in our early time-of-flight experiments and T. A. Carlson, G. Leibfried, O. S. Oen, and M. T. Robinson for their many helpful discussions during the course of this work.

[23] C. W. Nestor, T. C. Tucker, T. A. Carlson, L. D. Roberts, F. B. Malik, and C. Froese, Oak Ridge National Laboratory Report No. USAEC-ORNL 4027, 1966 (unpublished).

[24] See, e.g., E. Everhart and Q. C. Kessel, Phys. Rev. **146**, 16 (1966).

[25] B. R. Appleton, C. Erginsoy, and W. M. Gibson, Phys. Rev. **161**, 330 (1967).

[26] H. O. Lutz, S. Datz, C. D. Moak, T. S. Noggle, and L. C. Northcliffe, Bull. Am. Phys. Soc. **11**, 126 (1966).

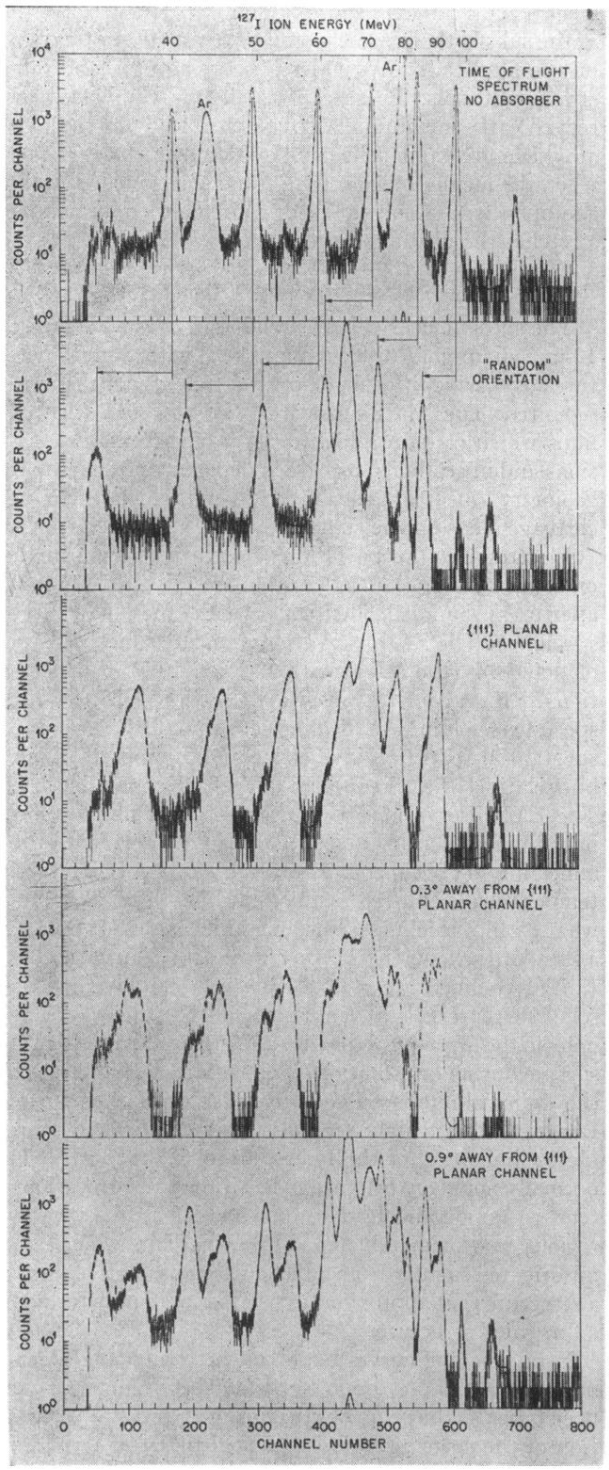


FIG. 3. Time-of-flight energy-loss spectra with multicomponent $^{127}$I beams through 0.3 $\mu$m of Au. Spectra are shown for random orientation and various tilt angles with respect to a {111} plane. The peaks labeled Ar arise from argon impurities in the stripper canal.